Solar Oscillation: Excitation, Damping and Line Asymmetry

尾崎洋二（東大天文）

1. はじめに

太陽振動　周期 ~ 5分

何千，何万の固有モード

音波の固有振動　p モード

日震学（helio-seismology）

振動を使って，太陽内部を探る研究

(1) 固有振動の振動数

逆問題

① 太陽内部での音速分布

② 内部の自転角速度分布

柴橋，関井

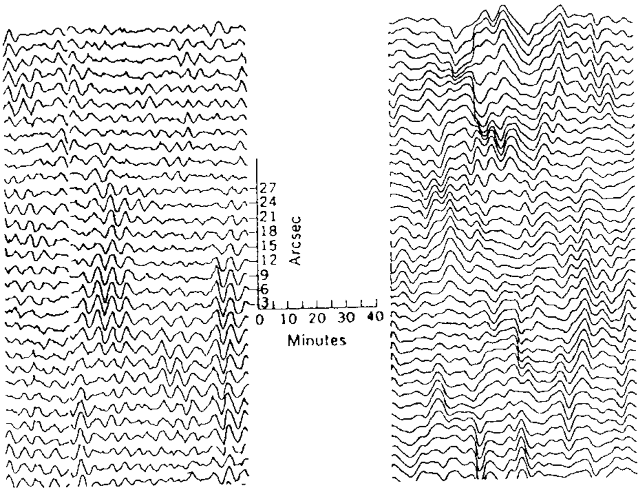

Fig. 11.1 (Left) Vertical velocity variation with time for points along a scan line on th solar surface separated by intervals of 3 arcsec (2.2 Mm) obtained by Musma and Rust (1970). The distance between the curves for adjacent points is equ to a velocity of 400 m s^{-1}. (Right) Intensity variation with time in the imag compressed into one dimension (5450 Å, FWHM of 400 Å) obtained b Nishikawa et al. (1986). Each curve is separated by 2.26 arcsec and 0.08% i the intensity fluctuation. (The radius of the sun is 0.696 × 10^6 km, and th angular diameter of the sun viewed from the earth is 32 arcmin. Thus, 1 arcse on the solar disk corresponds to 725 km; i.e., 1 arcsec = 0.725 Mm.)

(2) 励起 メカニズム

なぜ太陽は5分周期で振動するのか？

太陽基準振動周期 ～ 1時間

なぜ何千，何万という沢山のモードが励起されるのか？

観測情報

① モードの振巾

② line widths

③ line asymmetries

2. 励起メカニズム

① linear overstability

"脈動変光星"

② stochastic excitation

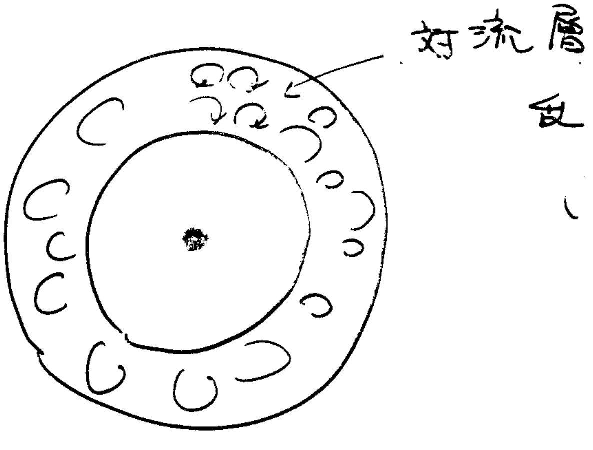

乱流からの音波の発

(Lighthill mechanis

太陽

音波の共鳴箱 (cavity)

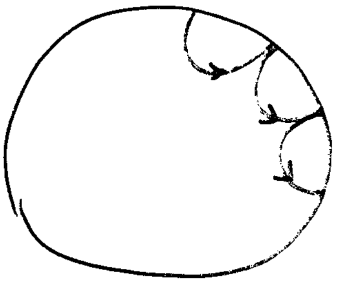

音波のパワースペクトル

共鳴箱のレスポ

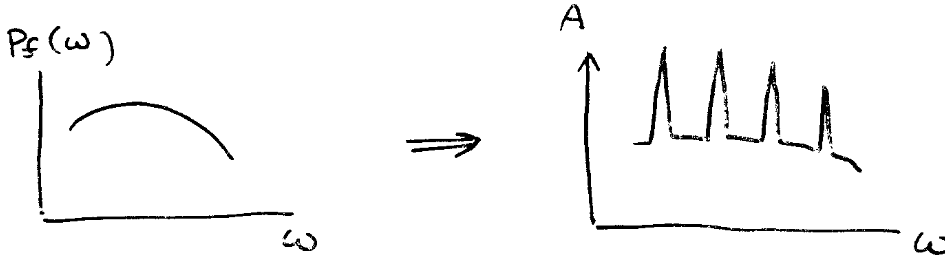

line の巾 $\longleftrightarrow$ $(\text{damping time})^{-1}$

$$\propto e^{i\omega_0 t - \gamma t}$$

レスポンス

振巾 $$|A|^2 = \frac{P_f(\omega)}{(\omega-\omega_0)^2 + 4\omega^2\gamma^2}$$

ローレンツ線輪郭

3 Stochastic Excitation of Solar Oscillations

excitation of solar oscillations

(1) linear overstability

(2) stochastic excitation

stochastic excitation of oscillations by
Goldreich and Keeley (1977)

the sun ······ "acoustic resonator"

eigenmode damped oscillator

$$v \propto \exp(i\ \omega_q\ t - \gamma_q\ t)$$

γ_q: **damping rate**

broad-band noise
generated by turbulent convection

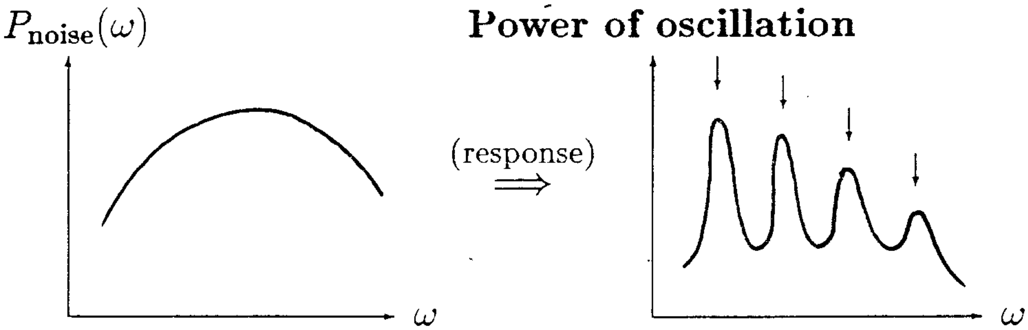

amplitude of ossilations

$$|A|^2 \propto \frac{P_{\rm noise}}{\gamma_q}$$

energy of a particular mode

$$\mathcal{E}_q = \left\langle \int_{M_\odot} v_q^2 dm \right\rangle$$

$$\frac{d\mathcal{E}_q}{dt} = \mathcal{G} - 2\gamma_q \mathcal{E}_q = \mathcal{G} - \Gamma \mathcal{E}_q$$

$\mathcal{G}$: **acoustic power available to a paticular mode**

$\Gamma = 2\gamma_q$: **energy damping rate (line width)**

steady state

$$\mathcal{G} = \Gamma \mathcal{E}_q$$

observations

(1) **amplitude of oscillations :** v_q
(eigen-function)
$\longrightarrow \mathcal{E}_q$

(2) **damping rate :** Γ **(line width)**
$\longrightarrow \mathcal{G}$**(observed)**

Libbrecht (1988)

Libbrecht (1988)

P-Mode Characteristics

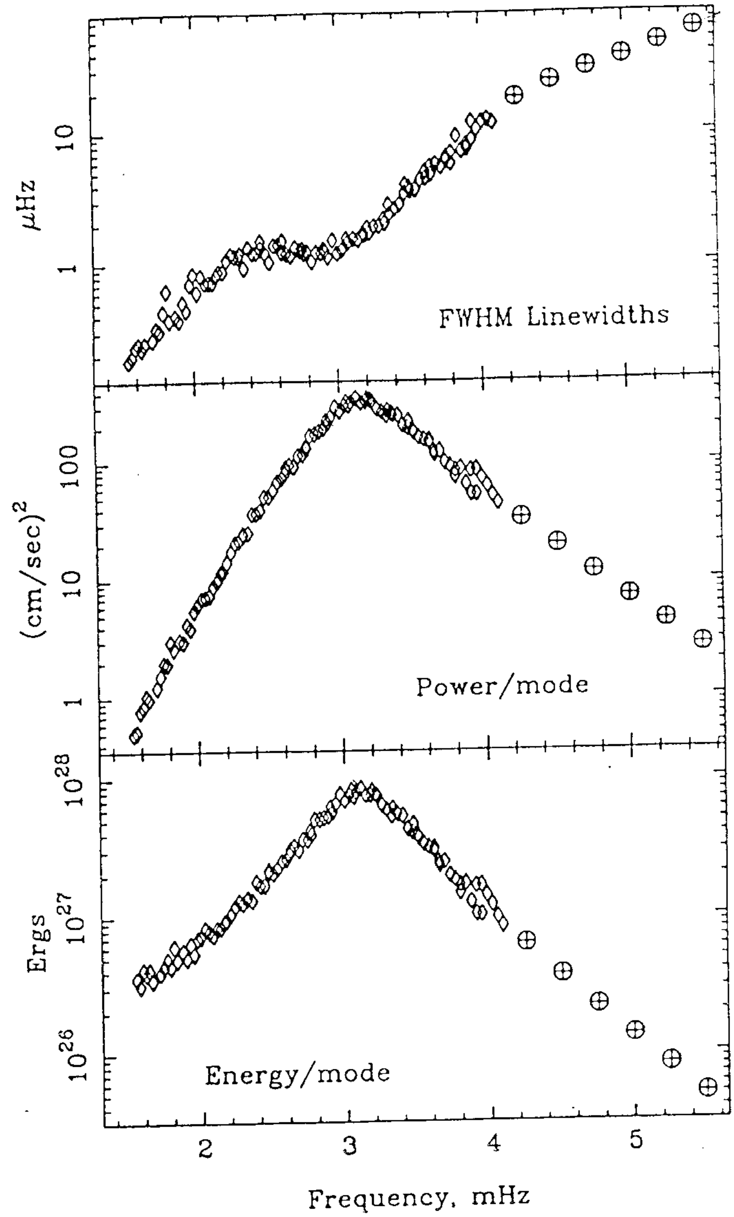

Figure 1. FWHM linewidths Γ, power per mode, and total energy (kinetic plus potential) per mode as a function of frequency, for low ℓ p-modes. The squares show fits from individual mode features with $\ell = 19$-24, while the circles are the result of a more indirect high frequency analysis of $\ell \simeq 60$ modes (Libbrecht 1988a). Power per mode is normalized to represent the mean square surface (radial) velocity per mode in (cm/sec)^2, averaged over time *and* over the solar surface. Because of an uncertain normalization of the Doppler images from which these results were derived, the overall normalization of the power could be in error by 10–20 percent. The energy per oscillation mode assumes the observations were made at $\tau_{5000} = 0.05$.

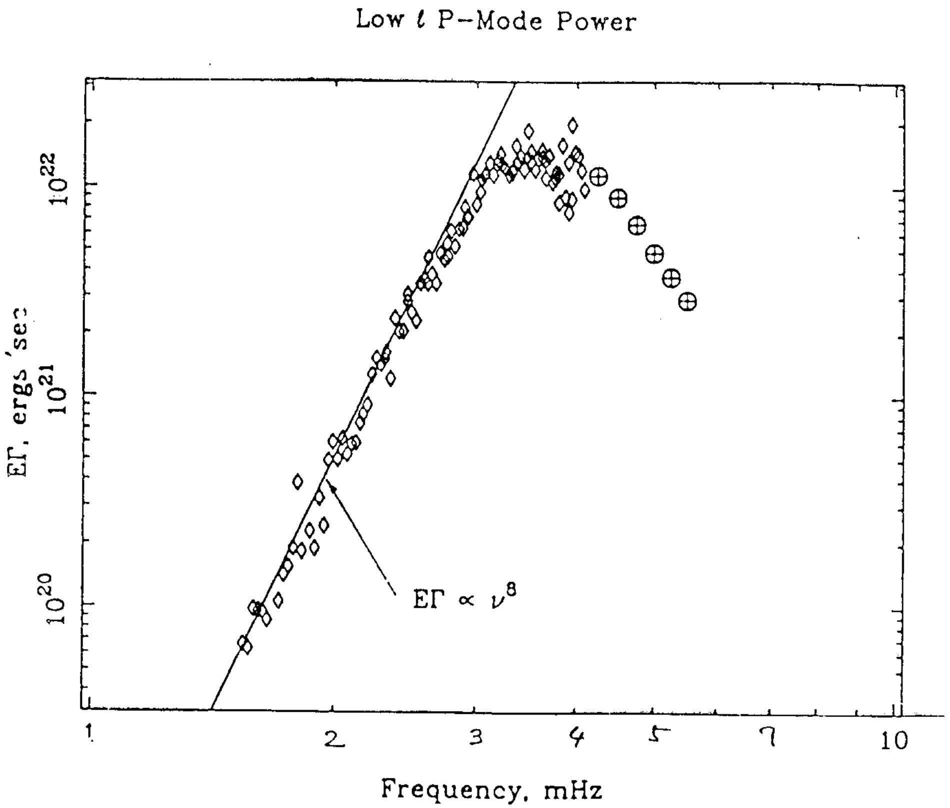

Figure 3. Log-log plot of $E\Gamma$, where E and Γ are separately plotted in Figure 1. This is equal to the power being pumped into the p-mode oscillators, presumably by convection. Note the high frequency cutoff, and the $\sim \nu^8$ falloff at low frequencies. This simple low frequency behavior is presently unexplained.

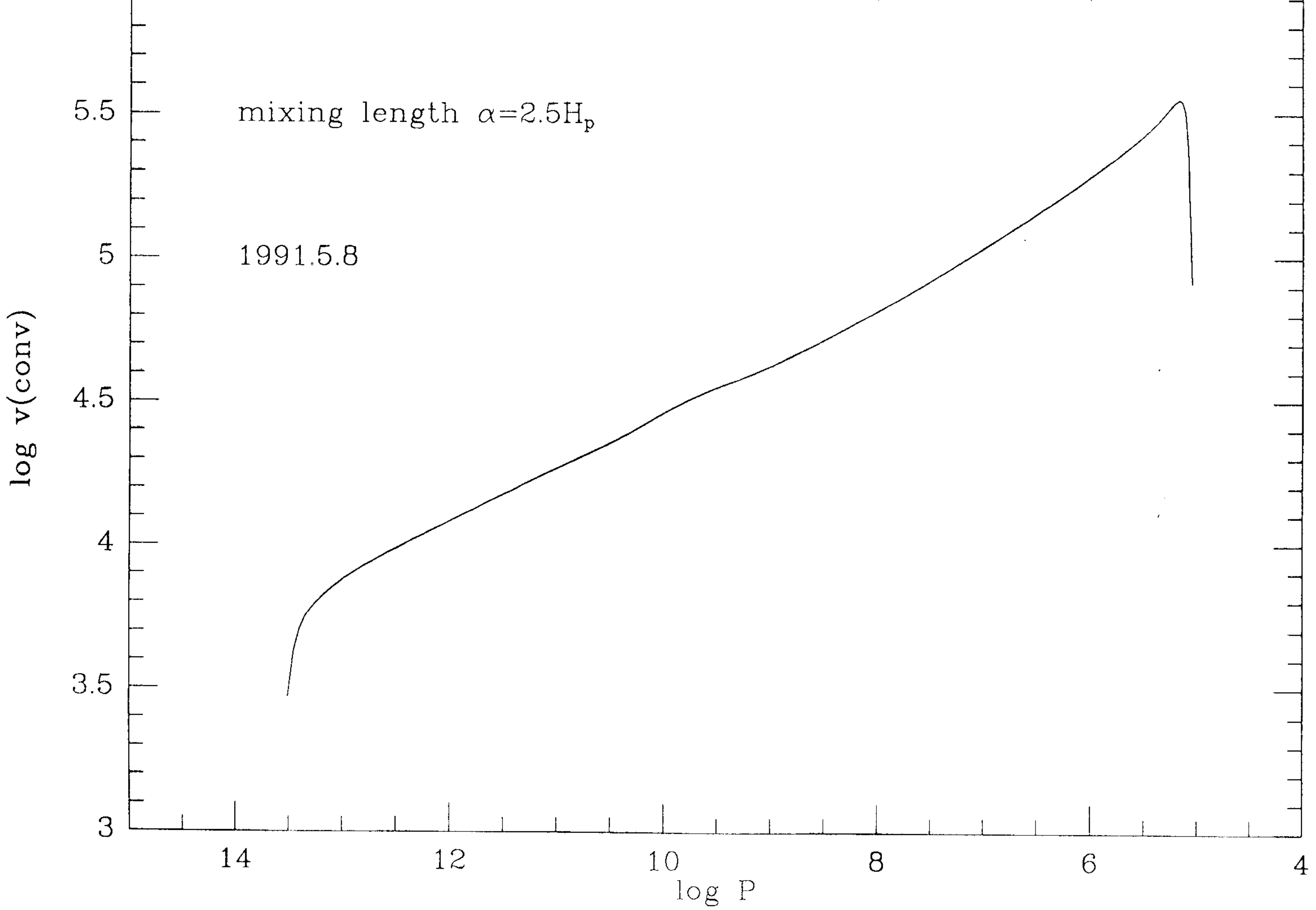
mixing length $\alpha=2.5H_p$
1991.5.8
log v(conv)
5.5
5
4.5
4
3.5
3
14
12
10
8
6
4
log P

Acoustic Noise Generation

Lighthill mechanism

turbulent eddy

size : λ **velocity :** v

density : ρ **Mach number :** $M = v/c$

acoustic power per unit volume :

$$\varepsilon \sim \frac{\rho v^3}{\lambda} M^{2n+1}$$

n: **multipole index**

$n = 2$ **"quadrupole radiation"**

$$\varepsilon \propto v^8$$

solar convection

acoustic emission from "transition zone"

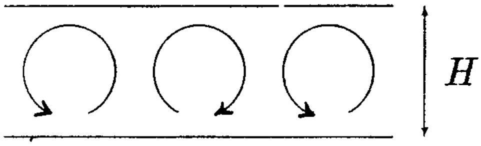

total power

$$P(\omega) \sim 4\,\pi\,R^2\,H\,\varepsilon(\omega)$$

$$\varepsilon(\omega) \sim \rho\ v_{\mathbf{max}}^2\ M^5 \begin{cases} (\omega/\omega_{\mathbf{Q}})^2 & \textbf{for} \quad \omega \leq \omega_{\mathbf{Q}} \\ (\omega/\omega_{\mathbf{Q}})^{-\underset{\nwarrow\, 7/2}{\cancel{7}}} & \textbf{for} \quad \omega \geq \omega_{\mathbf{Q}} \end{cases}$$

$\omega_{\mathbf{Q}}$**: resonance frequency**

$$\omega_{\mathbf{Q}} = 2\ \frac{\lambda}{v}$$

power per mode $\quad G_{\mathrm{s}}$

$$G_{\mathrm{s}} \sim P(\omega)\ \left(\frac{\Delta k}{k}\right)\ \Delta\omega$$

frequency band width

wave number band width

$$G_{\mathrm{s}} \sim \frac{\pi}{2}\ \left(\rho H^3\right)\ v^2\ M^3\ \Delta\omega \begin{cases} (\omega/\omega_{\mathbf{Q}})^0 & \textbf{for} \quad 0 \leq \omega \leq \\ (\omega/\omega_{\mathbf{Q}})^{-5.5} & \textbf{for} \quad \omega \geq \omega_{\mathbf{Q}} \end{cases}$$

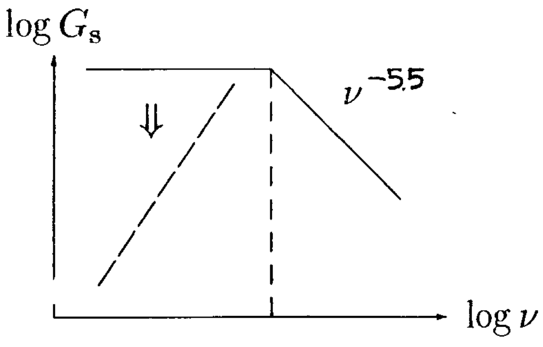

$\nu_{\mathbf{Q}} \sim$ **3.5mHz**

(1) high-frequency power

observations $G \propto \nu^{-5.3}$

theory $G \propto \nu^{-5.5}$
(quadrupole radiation)

(2) low-frequency power

$\nu < 3\mathrm{mHz}$

"attenuation" factor

$$G = G_s \ \exp(-\kappa \ d)$$
$$\propto \nu^{2n}$$

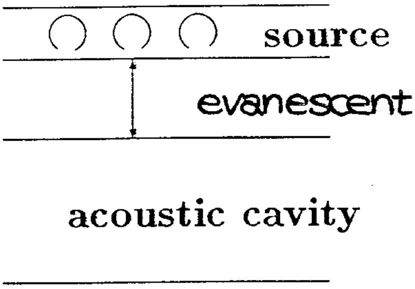
source
evanescent
acoustic cavity

n: effective polytropic index
$n \sim 4$

$$G \sim \nu^{8}$$

(3) numerical calculation

Goldreich and Keeley's (1977) formula

3. High Frequency Modes

太陽振動

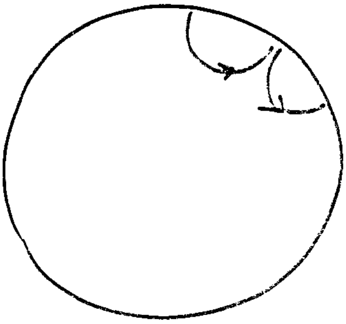

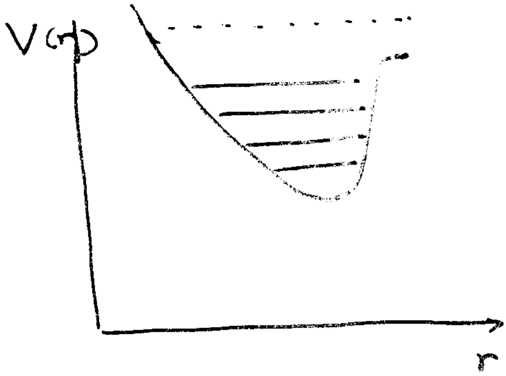

$$\frac{d^2\psi}{dr^2} + \left[\omega^2 - V\right]\psi = 0$$

acoustic cut-off frequency

$\nu_c \simeq 5.5$ mHz ⟷ 周期 180 sec

$\nu < \nu_c$ trapped waves
discrete eigenmodes

$\nu > \nu_c$ untrapped waves
continuum

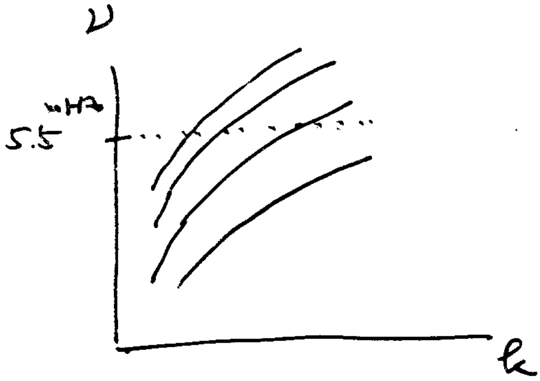

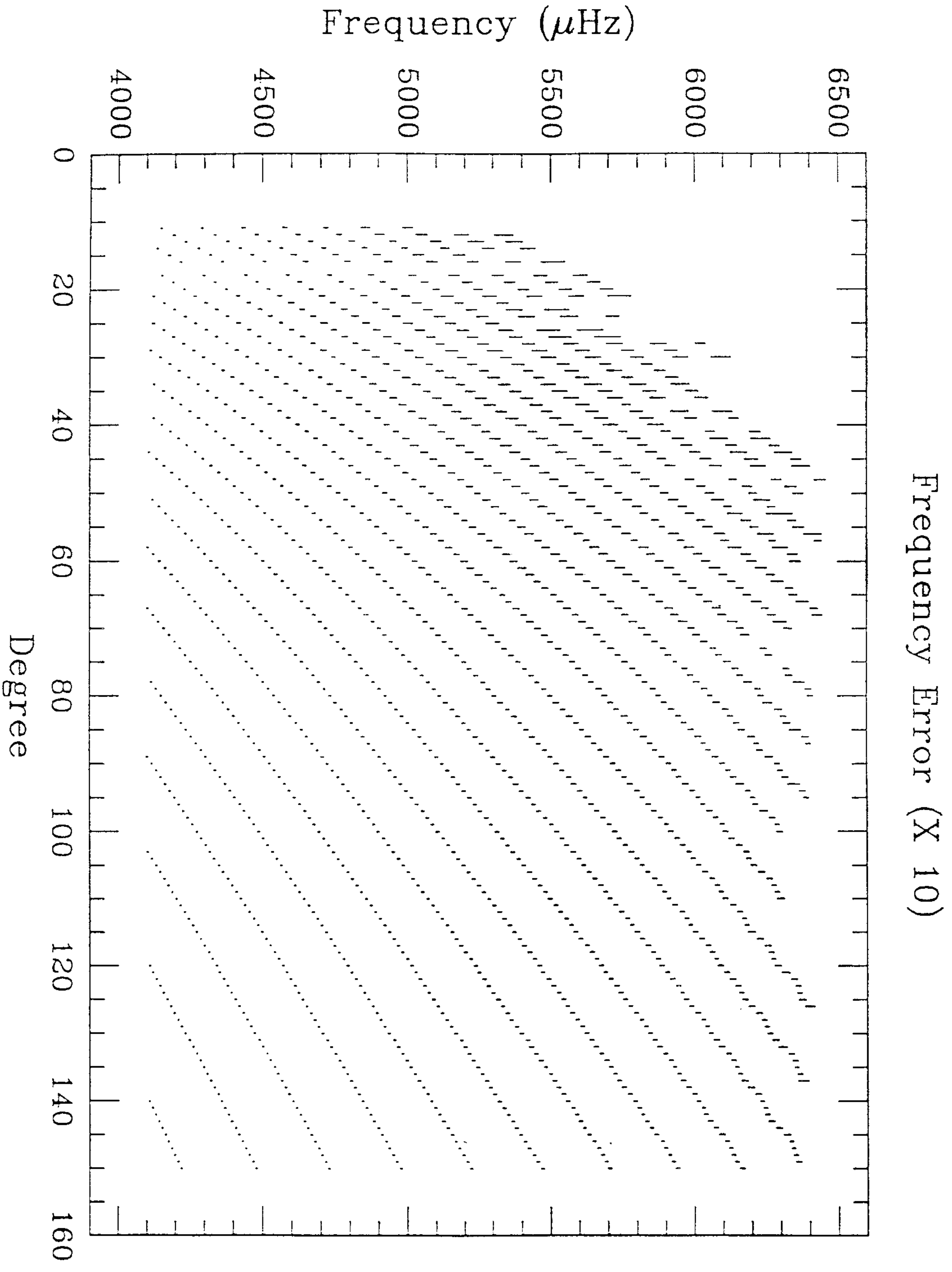
Frequency Error (X 10)
Frequency (μHz)
4000
4500
5000
5500
6000
6500
Degree
0
20
40
60
80
100
120
140
160

4. Leaky Cavity Model

high frequency modes について 2つの説明

① partial reflection モデル

Balmforth & Gough (1990)

② direct wave と reflected wave の

干渉パターン

P. Kumar (1990, 1991)

第2の立場 (leaky cavity model)

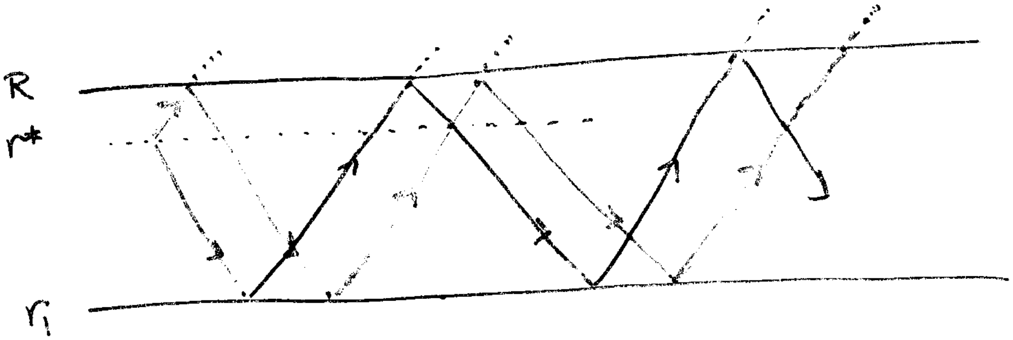

cavity の外側の境界で "部分反射"

反射係数 R

$$v_u(t) = A(\omega, l)\exp(i\omega t)\Big[\,1 + R\exp(-2i\Theta \\ R^2\exp(-4i\Theta) + \\ \cdots$$

phase $\Theta = \int_{r_1}^{R} k_r\,dr \quad \cdots(2)$

$$v_u(t) = A(\omega, l)\,\exp(i\omega t)\quad \frac{1}{1-R\,\exp(-2i}$$

次に downward wave について考える

$$v_d(t) = D\,A(\omega, l)\,\exp(i\omega t)\,\exp(-2i\theta^*)$$
$$[1 + R\exp(-2i\theta) + \cdots\cdots]$$

$$\boxed{\theta^* \equiv \int_{r_1}^{r^*} k_r\,dr}$$

音源と lower boundary との間の phase

$$= A(\omega, l)\,D\,\exp(-2i\theta^*)\,/\,[1 - R\,\exp(-2$$

$$v_u + v_d = A(\omega, l)\,\exp(i\omega t)\,\frac{1 + D\,\exp(-2i\theta^*)}{1 - R\,\exp(-2i\theta)}$$

観測されるパワースペクトル
$P(\omega)$

音源でのパワースペクトル $f(\omega)$

$$\boxed{P(\omega) = f(\omega)\,\frac{1 + D^2 + 2D\cos(2\theta^*)}{1 + R^2 - 2R\cos(2\theta)}}$$

$$f(\nu) \propto \nu^{-\beta}$$

[ex] Lighthill mechanism

$\beta = 5.5$

観測されるパワースペクトル

① $\nu \ll \nu_{ac}$

trapped mode $R \simeq 1$

量子条件

(1) の分母が最小

$\cos 2\theta = 1$ $2\theta = 2n\pi$

$$\theta = \int_{r_1}^{R} k_r \, dr = n\pi$$

線スペクトル

② $\nu \gtrsim \nu_{ac}$

$R \simeq 0$

$$P(\omega) = f(\omega) \left\{ 1 + D^2 + 2D \cos(2\theta^*) \right\}$$

スペクトルの peak

(1) の分子が最大

$$2\Theta^* = 2n\pi$$

量子条件

$$\Theta^* = \int_{r_1}^{r^*} k_r\,dr = n\pi$$

積分範囲に注意！

見かけ上 "cavity" が小さくなったように

振舞う。

$$\Theta^* = \theta - \delta = \int_{r_1}^{r^*} k_r\,dr = \omega\int_{r_1}^{r^*} \frac{dr}{c} = n\pi$$

$\uparrow$ "phase shift"

結論

① leaky cavity model

$\nu = \nu_{ac}$ をはさんで 連続して "ridge"

② シミュレーション

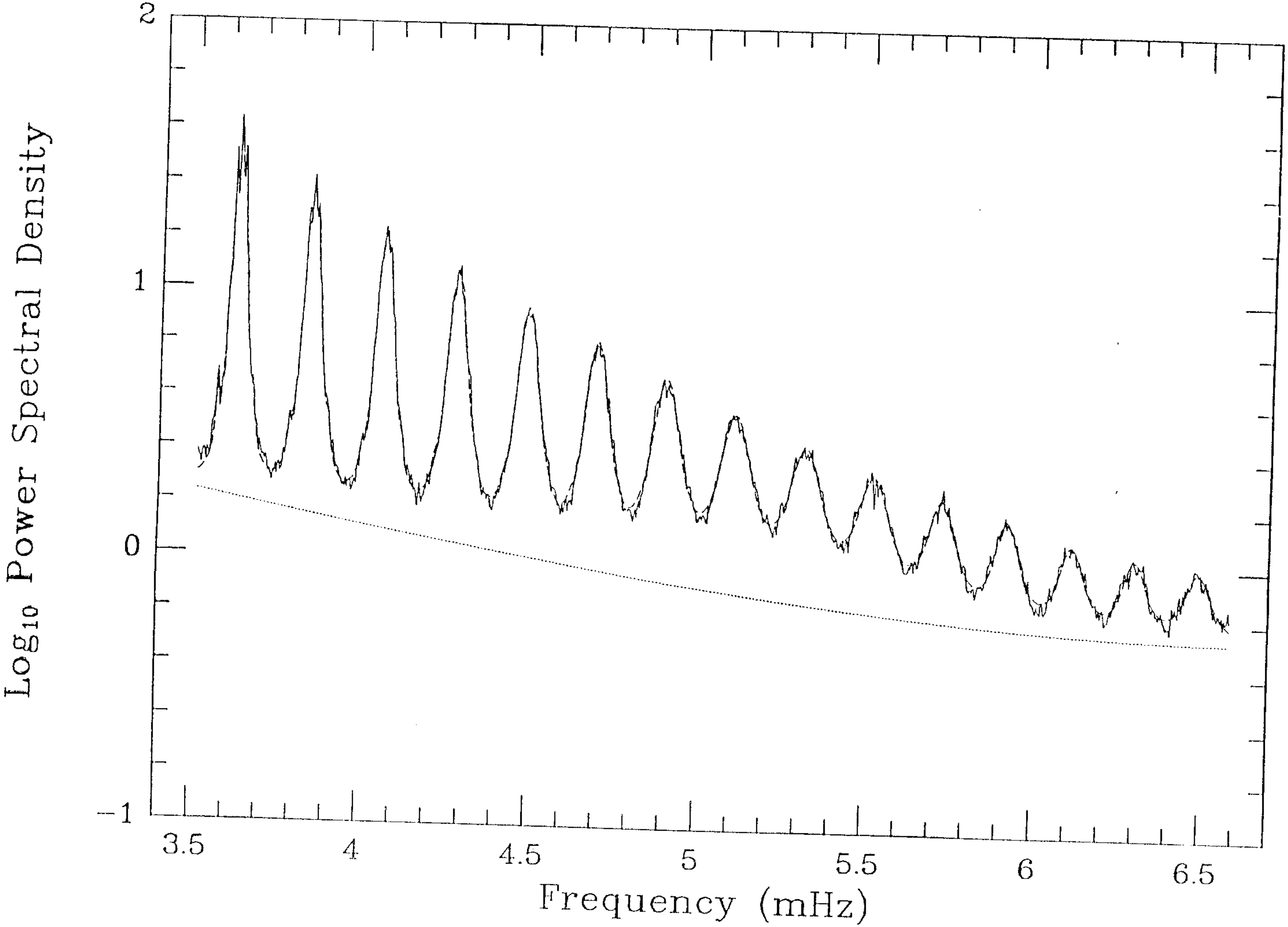

Fit of Model to Data

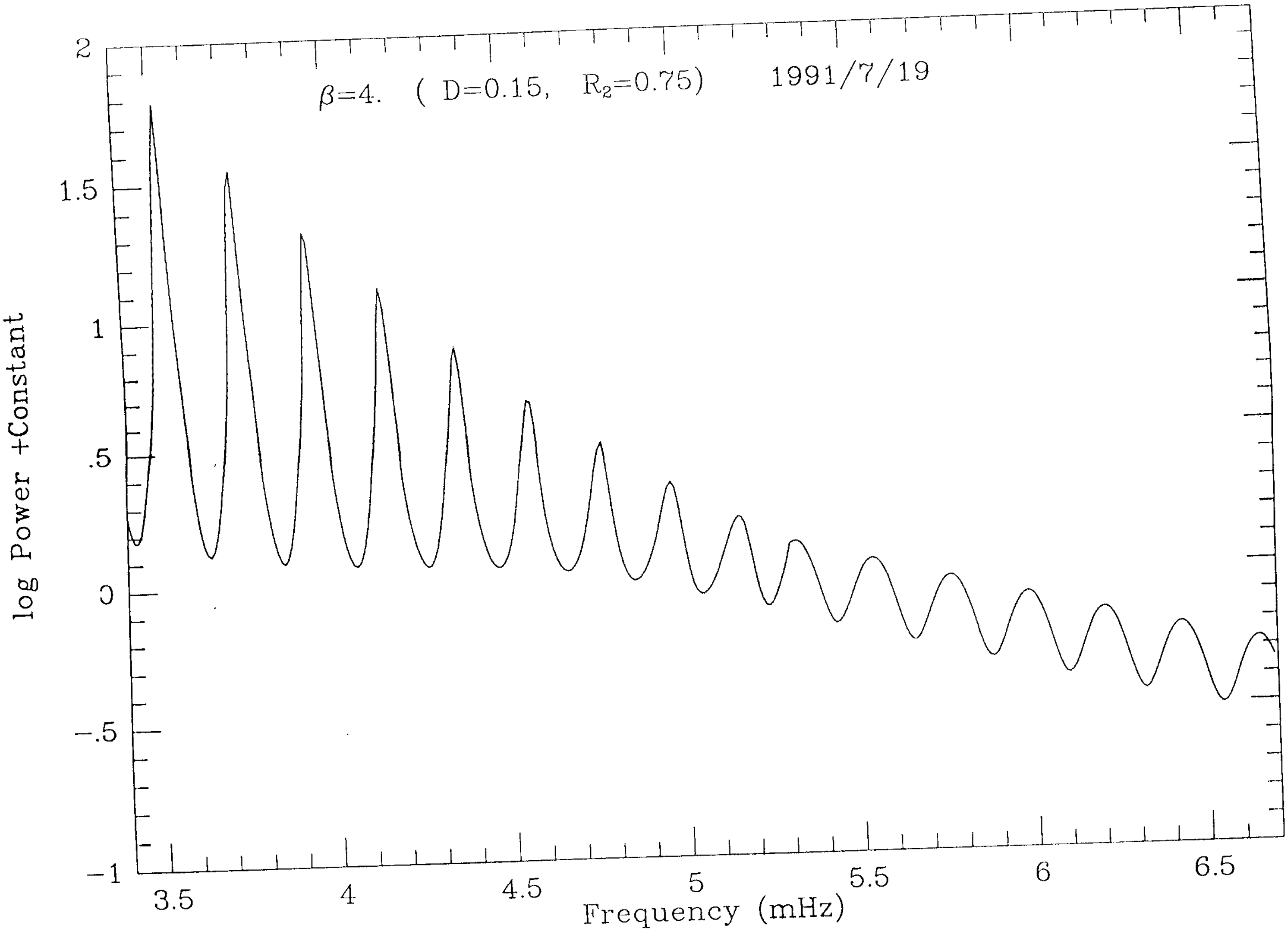
β=4. (D=0.15, R_2=0.75) 1991/7/19
log Power +Constant
2
1.5
1
.5
0
-.5
-1
3.5
4
4.5
5
5.5
6
6.5
Frequency (mHz)

5. Line Asymmetries

これまでの観測のパワースペクトル

ローレンツ線輪郭

Duvall, et. al. (Ap. J., 410, 829, 1993)

line asymmetries の発見

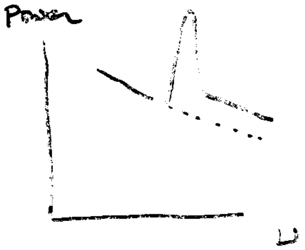

line asymmetries の説明

leaky cavity モデル

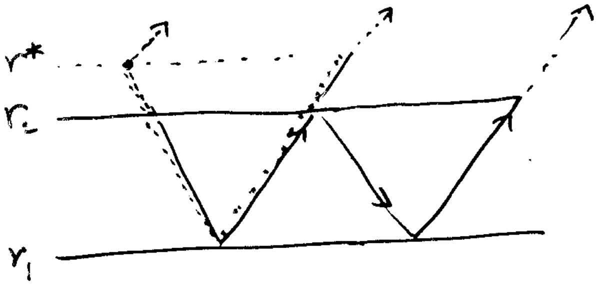

$$v_u(t) = A(\omega, l)\, e^{i\omega t}$$

$$v_d(t) = D A(\omega, l) \exp\ i(\omega t - 2\theta + 2\delta\theta$$

$$[\,1 + R \exp(2i\theta) + R^2 \exp($$

$$+ \cdots]$$

$$v(t) = A(\omega, l)\exp(i\omega t)$$

$$\left[\ 1 + \frac{D\exp(-2i\theta^*)}{1 - R\exp(-2i\theta)}\right]$$

phase shift $\delta\theta$ $\Longleftrightarrow$ asymmetry

asymmetry の観測 $f(\nu, \cancel{\ell})$

$\approx 10\%$ at the lowest frequency

$(\nu \sim 2\mathrm{mHz})$

$\approx 0\ \%$ $(\nu \simeq 3.2\mathrm{mHz})$

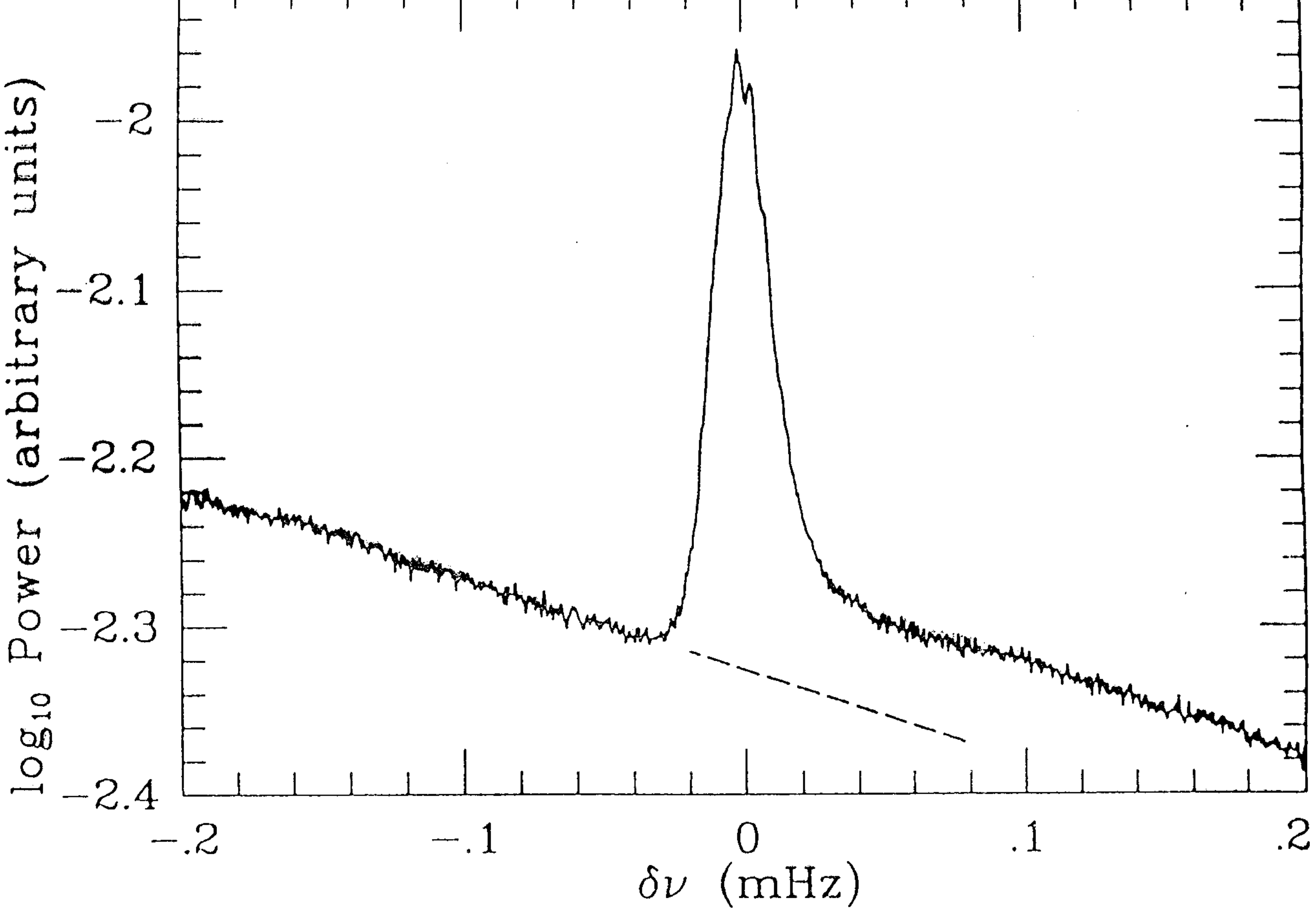

FIG. 1.—Average power spectrum for modes of radial order $n = 2$, and spherical harmonic degree $l = 157$–221 for the 1988 South Pole data. The frequency dependences on azimuthal order m and degree l were removed before averaging. Solid line indicates the data. Dashed line indicates a linear extension of the background from the low-frequency side of the peak.

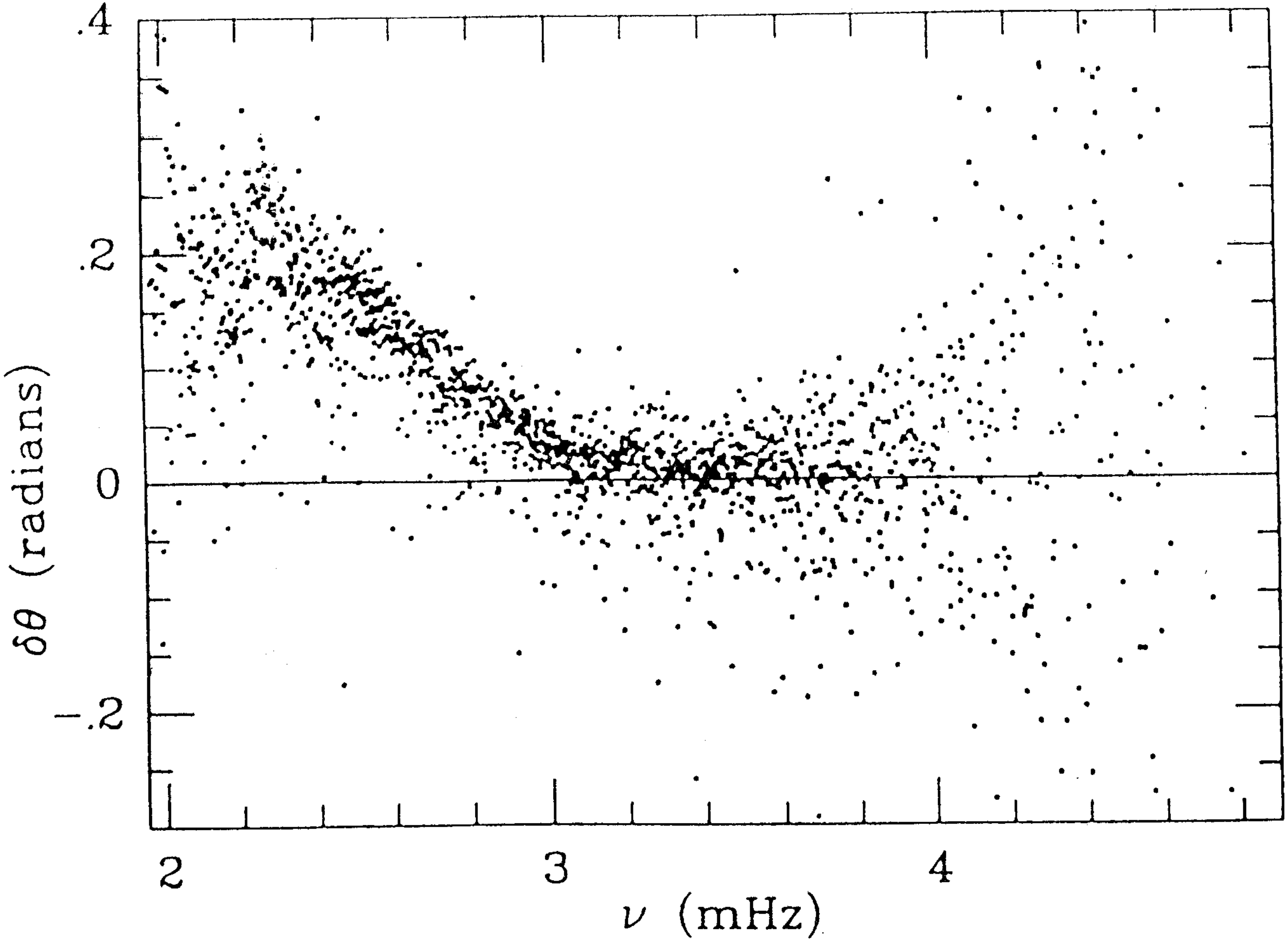

FIG. 3.—$\delta\theta$ from fits to the 1988 South Pole data ($0 < l \leq 170$). A positive value represents additional phase shift between the acoustic noise source and the top of the resonant cavity.

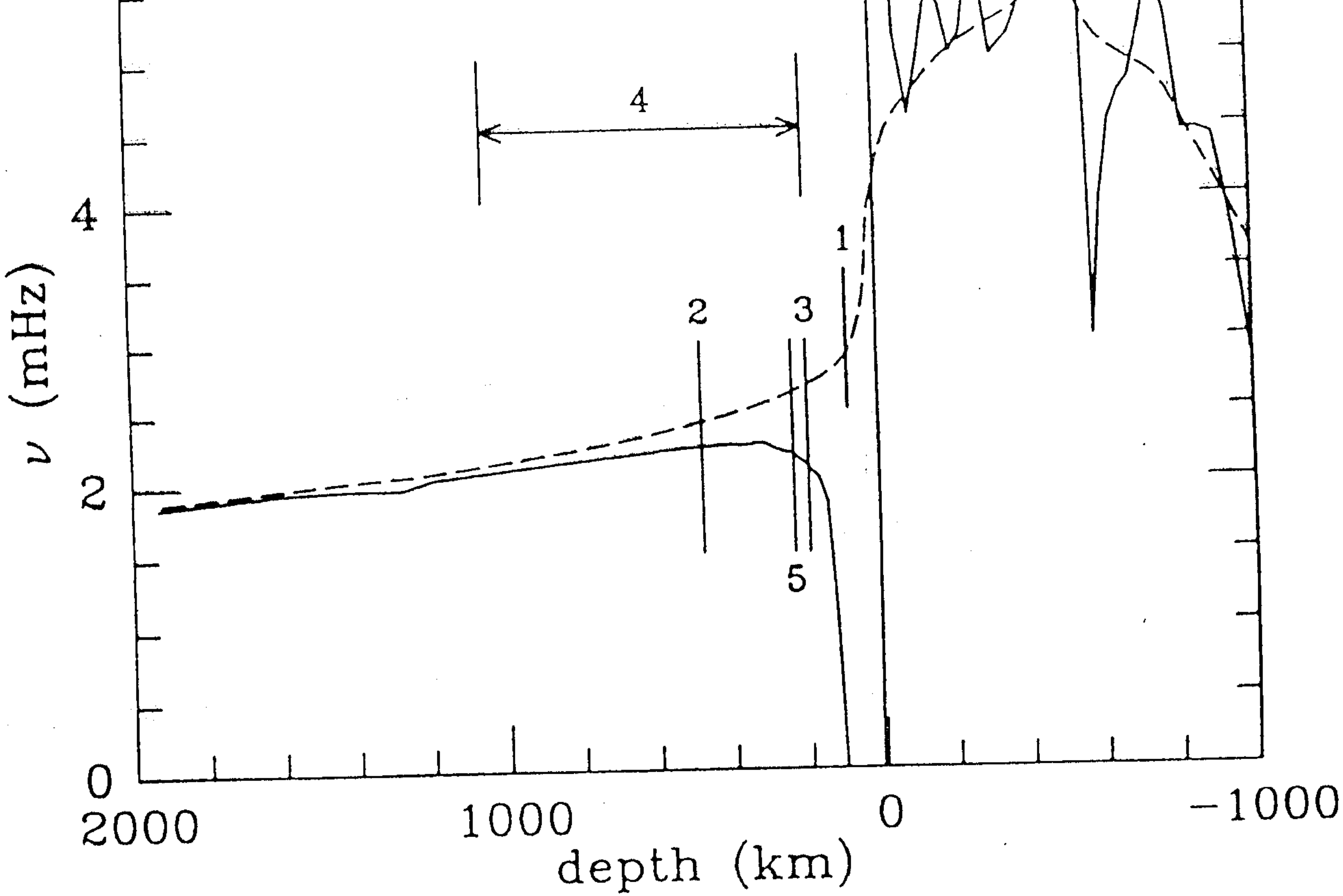

FIG. 6.—Acoustic cutoff frequency versus depth in the solar envelope. Solid line represents calculations based on the density scale height, and the dashed line represents calculations based on the pressure scale height. Several depths are marked at which different authors placed the acoustic generation region (1–5). These are referred to in the text.